Article

1-Adamantanethiolate Monolayer Displacement Kinetics Follow a Universal Form

Hctor M. Saavedra, Corina M. Barbu, Arrelaine A. Dameron, Thomas J. Mullen, Vincent H. Crespi, and Paul S. Weiss

J. Am. Chem. Soc., **2007**, 129 (35), 10741-10746• DOI: 10.1021/ja071116z • Publication Date (Web): 09 August 2007

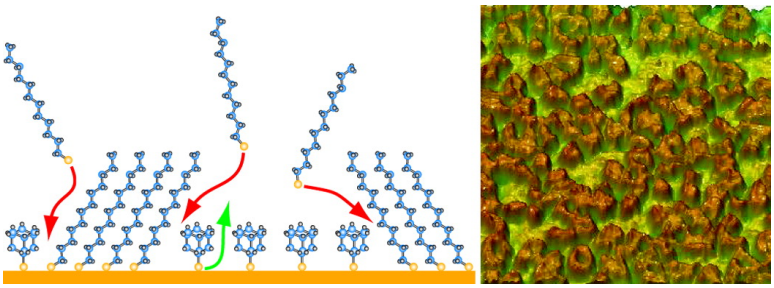

More About This Article

Additional resources and features associated with this article are available within the HTML version:

- Supporting Information
- Links to the 5 articles that cite this article, as of the time of this article download
- Access to high resolution figures
- Links to articles and content related to this article
- Copyright permission to reproduce figures and/or text from this article

View the Full Text HTML

J|A|C|S
ARTICLES
Published on Web 08/09/2007

1-Adamantanethiolate Monolayer Displacement Kinetics Follow a Universal Form

Héctor M. Saavedra,[†,‡] Corina M. Barbu,[‡] Arrelaine A. Dameron,[†,‡] Thomas J. Mullen,[†,‡] Vincent H. Crespi,*[,‡] and Paul S. Weiss*[,†,‡]

Contribution from the Departments of Chemistry and Physics, The Pennsylvania State University, 104 Davey Laboratory, University Park, Pennsylvania 16802-6300

Received February 20, 2007; E-mail: stm@psu.edu (P.S.W.); vhc2@psu.edu (V.H.C.)

Abstract: Alkanethiol molecules in solution displace 1-adamantanethiolate self-assembled monolayers on Au{111}, ultimately leading to complete molecular exchange. Specifically, here, fast insertion of *n*-dodecanethiolate at defects in the original 1-adamantanethiolate monolayer nucleates an island growth phase, which is followed by slow ordering of the *n*-dodecanethiolate domains into a denser and more crystalline form. Langmuir-based kinetics, which describe alkanethiolate adsorption on bare Au{111}, fail to model this displacement reaction. Instead, a Johnson−Mehl−Avrami−Kolmogorov model of perimeter-dependent island growth yields good agreement with kinetic data obtained by Fourier transform infrared spectrometry over 100-fold variation in *n*-dodecanethiol concentration. Rescaling the growth rate at each concentration collapses all the data onto a single universal curve, suggesting that displacement is a scale-free process. The rate of displacement varies as the square-root of the *n*-dodecanethiol concentration across the 0.01−1.0 mM range studied.

1. Introduction

The patterning and functionalization of surfaces with self-assembled monolayers (SAMs) facilitate the creation of complex well-ordered structures for biosensors,[1] biomimetics,[2,3] molecular electronics,[4,5] lithography,[6−9] and other applications.[10] However, surface diffusion and contamination hinder the creation of high-quality structures, especially for soft-lithographic techniques that require multiple deposition steps. Protective layers can assist in controlling deposition, if they can be easily removed when desired but otherwise remain impermeable during the fabrication of surface-bound nanoscale assemblies.

We have recently demonstrated that 1-adamantanethiolate (**AD**) SAMs are labile and can be displaced by short-chain *n*-alkanethiolates.[11] Although such displacement or exchange reactions are not unique to **AD** SAMs, the complete and rapid displacement of one SAM by another under gentle thermal conditions (room temperature) and dilute concentrations (millimolar) is highly unusual.[12−14] The labile nature of **AD** SAMs makes possible micro-displacement printing, a technique similar to micro-contact printing but wherein the patterned molecules displace an existing SAM in only stamped regions and the remaining SAM acts as both a place-holder and a diffusion barrier.[7,8] These diffusion barriers not only create sharper, higher quality patterns but also extend the library of patternable molecules to those otherwise too mobile to retain surface patterns. This is extremely useful when patterning molecules with useful conducting or sensing properties that do not form robust SAMs as do unfunctionalized long-chain alkanethiolates. The same methodology can be used to improve other chemical patterning techniques, such as dip-pen nanolithography,[15] for which the applications range from lithographic resists[16] to biologically compatible surfaces[17,18] and proteomics.[19] However,

[†] Department of Chemistry.
[‡] Department of Physics.

(1) Huang, L.; Reekmans, G.; Saerens, D.; Friedt, J. M.; Frederix, F.; Francis, L.; Muyldermans, S.; Campitelli, A.; Van Hoof, C. *Biosens. Bioelectron.* **2005**, *21*, 483−490.
(2) Kwok, C. S.; Mourad, P. D.; Crum, L. A.; Ratner, B. D. *Biomacromolecules* **2000**, *1*, 139−148.
(3) Mullen, T. J.; Dameron, A. A.; Andrews, A. M.; Weiss, P. S. *Aldrichim. Acta* **2007**, *40*, 21−31.
(4) Mantooth, B. A.; Weiss, P. S. *Proc. IEEE* **2003**, *91*, 1785−1802.
(5) Moore, A. M.; Dameron, A. A.; Mantooth, B. A.; Smith, R. K.; Fuchs, D. J.; Ciszek, J. W.; Maya, F.; Yao, Y. X.; Tour, J. M.; Weiss, P. S. *J. Am. Chem. Soc.* **2006**, *128*, 1959−1967.
(6) Anderson, M. E.; Mihok, M.; Tanaka, H.; Tan, L. P.; Horn, M. W.; McCarty, G. S.; Weiss, P. S. *Adv. Mater.* **2006**, *18*, 1020−1022.
(7) Dameron, A. A.; Hampton, J. R.; Smith, R. K.; Mullen, T. J.; Gillmor, S. D.; Weiss, P. S. *Nano Lett.* **2005**, *5*, 1834−1837.
(8) Dameron, A. A.; Hampton, J. R.; Gillmor, S. D.; Hohman, J. N.; Weiss, P. S. *J. Vac. Sci. Technol. B* **2005**, *23*, 2929−2932.
(9) Smith, R. K.; Lewis, P. A.; Weiss, P. S. *Prog. Surf. Sci.* **2004**, *75*, 1−68.
(10) Mullen, T. J.; Srinivasan, C.; Hohman, J. N.; Gillmor, S. D.; Shuster, M. J.; Horn, M. W.; Andrews, A. M.; Weiss, P. S. *Appl. Phys. Lett.* **2007**, *90*, 063114.
(11) Dameron, A. A.; Charles, L. F.; Weiss, P. S. *J. Am. Chem. Soc.* **2005**, *127*, 8697−8704.
(12) Kassam, A.; Bremner, G.; Clark, B.; Ulibarri, G.; Lennox, R. B. *J. Am. Chem. Soc.* **2006**, *128*, 3476−3477.
(13) Lussem, B.; Muller-Meskamp, L.; Karthauser, S.; Waser, R.; Homberger, M.; Simon, U. *Langmuir* **2006**, *22*, 3021−3027.
(14) Schlenoff, J. B.; Li, M.; Ly, H. *J. Am. Chem. Soc.* **1995**, *117*, 12528−12536.
(15) Pener, R. D.; Zhu, J.; Xu, F.; Hong, S.; Mirkin, C. A. *Science* **1999**, *283*, 661−663.
(16) Weinberger, D. A.; Hong, S.; Mirkin, C. A.; Wessels, B. W.; Higgins, T. B. *Adv. Mater.* **2000**, *12*, 1600−1603.
(17) Lee, K. B.; Park, S. J.; Mirkin, C. A.; Smith, J. C.; Mrksich, M. *Science* **2002**, *295*, 1702−1705.
(18) Cheung, C. L.; Camarero, J. A.; Woods, B. W.; Lin, T. W.; Johnson, J. E.; De Yoreo, J. J. *J. Am. Chem. Soc.* **2003**, *125*, 6848−6849.
(19) Barbulovic-Nad, I.; Lucente, M.; Sun, Y.; Zhang, M. J.; Wheeler, A. R.; Bussmann, M. *Crit. Rev. Biotechnol.* **2006**, *26*, 237−259.

little is known about the kinetics of **AD** SAM displacement—understanding these kinetics is important to achieve higher quality, reproducible chemically patterned films and to guide the design of new molecules for use as selectively labile monolayers.

X-ray photoelectron spectroscopy has shown that **AD** and *n*-alkanethiolate SAMs have similar 2p sulfur chemical environments,[20] so the displacement is not due to differences in Au−S bond strengths. Scanning tunneling microscopy (STM) has shown that *n*-alkanethiolate SAMs are 1.8 times denser than **AD** SAMs.[21] This density difference provides a substantial enthalpic driver, aided by differences in van der Waals forces, to displace the **AD** SAMs completely. Imaging with STM reveals that displacement begins with a rapid nucleation phase, where *n*-dodecanethiolate (**C12**) molecules insert at defect sites of the **AD** SAM, followed by radial growth into domains that coalesce and eventually fully displace the original monolayer.[22] The defects consist of both randomly distributed single-atom-deep vacancy islands in the gold substrate (from lifting the Au{111} surface reconstruction during self-assembly)[23−25] and rotational/tilt domain boundaries in the original SAM. Here, we use Fourier transform infrared spectrometry (FTIR) to study the quantitative kinetics of the solution-phase displacement of **AD** SAMs by **C12** on Au{111}.

2. Experimental Methods

n-Dodecanethiol from Sigma-Aldrich (St. Louis, MO) was used as received. 1-Adamantanethiol and perdeuterated *n*-dodecanethiol were synthesized by methods previously described.[11] Ethanol (200-proof) from Pharmaco (Brookfield, CT) was used as received. Monolayers were fabricated by immersing flame-annealed Au{111} on mica substrates (Molecular Imaging, Tempe, AZ) into ethanolic solutions of the desired thiol molecule. Perdeuterated *n*-dodecanethiolate SAMs (used for normalization of the FTIR signals) were prepared from 1.0 mM solutions, while the **AD** SAMs were prepared from 10 mM solutions. After 24 h deposition from solution, the gold substrates were removed, rinsed with 200-proof ethanol, and dried under a stream of nitrogen. All **AD** SAMs were used immediately after preparation.

Infrared spectra were collected using a Nicolet 6700 FTIR spectrometer (Thermo Electron Corp., Waltham, MA), equipped with a liquid-nitrogen-cooled mercury−cadmium−telluride detector and a Seagull variable-angle reflection accessory (Harrick Scientific Inc., Ossining, NY). The spectrometer and its accessory were purged with dry and CO_2-free air produced from a FTIR Purge Gas Generator (Parker-Balston, Cleveland, OH). The data were collected at grazing incidence reflection (84° relative to the surface normal) with p-polarized light and a mirror speed of 1.27 cm/s, with a resolution of 2 cm^{-1}. The first and last spectra, 0 min and 24 h, were averaged over 1024 scans, while all the spectra for the kinetic measurements were averaged over 400 scans. All SAM spectra were transformed using N−B medium apodization and normalized with data recorded for perdeuterated *n*-dodecanethiolate monolayers on Au{111}.

Prior to displacement, FTIR spectra were acquired for each **AD** SAM to verify the absence of impurity-related features and the presence of the CH_2 stretch at 2911 ± 1 cm^{-1}, both indicative of a well-ordered **AD** SAM.[22,26] The samples were then placed in ethanolic **C12** solutions of the specified concentration to achieve displacement. Every 6 min, the SAMs were rinsed with ethanol and dried with nitrogen, a FTIR spectrum was recorded, and the sample was returned to the **C12** solution for the next incremental exposure. Once the signals plateaued, displacements were no longer incrementally monitored. However, in order to achieve saturation coverage, the samples were placed in a **C12** solution overnight to allow for slow reordering and annealing. Subsequently, a final spectrum was recorded for each sample.

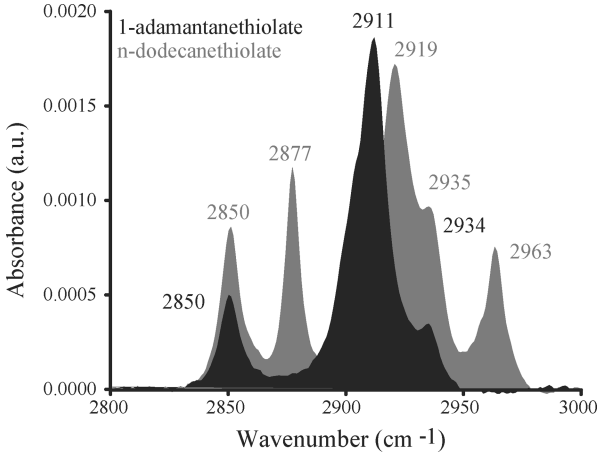

Figure 1. Infrared spectra of the C−H stretch region of a **AD** SAM (black) and a **C12** SAM (gray), showing their spectral overlap (see text for mode assignments).

3. Results and Discussion

Grazing incidence infrared reflection spectra of adsorbed species were obtained from 400 to 4000 cm^{-1}. The region from 2800 to 3000 cm^{-1} contains the CH_2 and CH_3 stretch modes of the aliphatic and carbon-cage tails of the thiolated molecules. Figure 1 shows typical spectra of an **AD** SAM (black) and a **C12** SAM (gray), both recorded after 24 h solution deposition. Several absorption peaks overlap in this region: CH_2 symmetric stretches (2850 cm^{-1} for both **AD** and **C12** SAMs) and CH_2 asymmetric stretches (2911 cm^{-1} for **AD** SAMs and 2919 cm^{-1} for **C12** SAMs).[26] The peaks that do not overlap correspond to the CH_3 symmetric and asymmetric stretching modes of the **C12** SAM, at 2877 and 2963 cm^{-1}, respectively.[27]

The spectra in Figure 2A provide peak intensities and positions as a function of immersion time and solution concentration. Figure 2A displays four spectra obtained at increasing immersion times in a 0.11 mM **C12** solution; each is a sum of contributions from both **AD** and **C12**. Figure 2B plots the integrated 2877 cm^{-1} peak intensity as a function of exposure time. Molecular orientation and lattice crystallinity affect the spectrum; for example, shifts in the CH_2 asymmetric mode track monolayer order and crystallinity. However, the symmetric and asymmetric CH_3 stretching modes are not sensitive to the orientation of the **C12** molecule, because of the tetrahedral coordination of the three relevant hydrogens. Therefore, the strength of the symmetric CH_3 mode directly measures the **C12** surface coverage.[27] Initially, this mode is very weak. After about 18 min of exposure to 0.11 mM **C12**, the intensity of the 2877 cm^{-1} peak increases rapidly and eventually dominates the spectrum. After 36 min, no signal from **AD** molecules can be detected by FTIR, and the spectrum is nearly identical to that

(20) Dameron, A. A.; Mullen, T. J.; Hengstebeck, R. W.; Saavedra, H. M.; Weiss, P. S. *J. Phys. Chem. C* **2007**, *111*, 6747−6752.
(21) Mullen, T. J.; Dameron, A. A.; Weiss, P. S. *J. Phys. Chem. B* **2006**, *110*, 14410−14417.
(22) Mullen, T. J.; Dameron, A. A.; Saavedra, H. M.; Williams, M. E.; Weiss, P. S. *J. Phys. Chem. C* **2007**, *111*, 6740−6746.
(23) Poirier, G. E. *Chem. Rev.* **1997**, *97*, 1117−1127.
(24) Poirier, G. E. *Langmuir* **1997**, *13*, 2019−2026.
(25) Poirier, G. E.; Pylant, E. D. *Science* **1996**, *272*, 1145−1148.
(26) Jensen, J. O. *Spectrochim. Acta, Part A* **2004**, *60*, 1895−1905.
(27) Nuzzo, R. G.; Dubois, L. H.; Allara, D. L. *J. Am. Chem. Soc.* **1990**, *112*, 558−569.

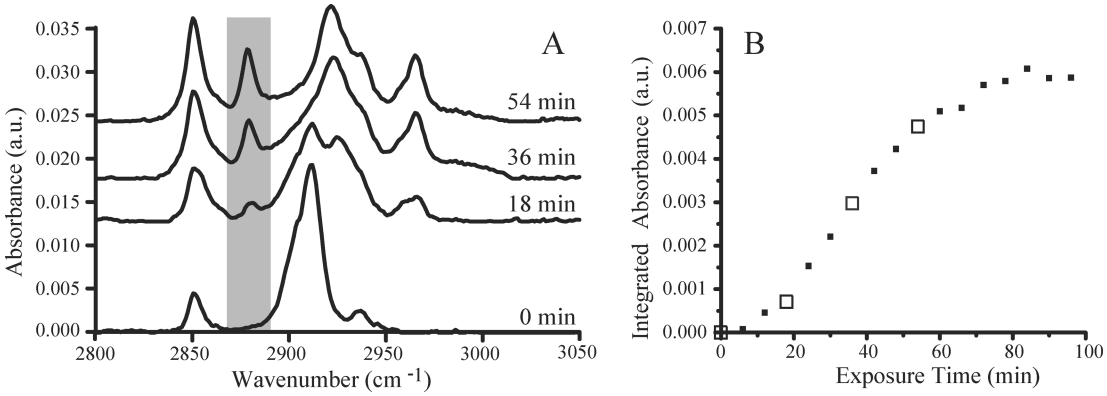

Figure 2. (A) Representative FTIR spectra of a 0.11 mM **C12** solution displacing an **AD** SAM. The 2877 cm^{-1} peak, corresponding to the CH_3 symmetric mode, is highlighted. (B) Kinetic curve derived from the FTIR spectra by plotting the integrated **C12** CH_3 symmetric mode peak versus deposition exposure time. The open squares represent the integrated absorbance for each of the four spectra shown on the left.

of a pure **C12** SAM. Displacement becomes very slow at around 92% of the final saturation intensity and approaches final saturation only after 24 h in solution. A similar but faster time evolution is observed at higher displacement solution concentrations.

Ellipsometry,[28] surface acoustic wave devices,[29] second harmonic generation,[30,31] and quartz crystal microbalance[32] measurements have established that the growth rates of alkanethiolate monolayers on bare Au{111} surfaces are proportional to the number of unoccupied adsorption sites on the surface, i.e., follow Langmuir kinetics. We consider seven kinetic models for **C12**/**AD** displacement kinetics: a model based on pure diffusion, four variants of simple Langmuir kinetics, and two models based on island growth.

For diffusion-controlled adsorption, the time-dependent coverage follows from the solution of the diffusion equations for a semi-infinite medium:[14,33]

$$\theta(t) = \sqrt{\kappa_D t}\,, \tag{1}$$

where

$$\kappa_D = \frac{4D}{\pi B_{ml}^2}\,, \tag{2}$$

D is the diffusion constant and B_{ml} is the number of molecules per unit area in the full monolayer. The rate of adsorption is then proportional to the flux of molecules to the surface. Since this model does not account for saturation or the depletion of adsorption sites, it could only apply to the initial stages of growth.

First-order Langmuir kinetics assume an irreversible random process with a rate proportional to the number of unoccupied adsorption sites:[34]

$$\theta(t) = 1 - e^{-\kappa t}\,, \tag{3}$$

where θ is the surface coverage and κ is the rate constant. In this model, the adsorption rate is uniform across the entire available surface, since the model assumes equivalent surface sites and no interactions with pre-adsorbed or solvent molecules.

Despite their simplicity, first-order Langmuir kinetics describe monolayer uptake curves on bare gold surfaces fairly well. They have also been used to model the molecular exchange of *n*-octadecanethiolate SAMs by radiolabeled *n*-octadecanethiol molecules, although the reaction took 50 h and reached only ~60% completion.[14] If the onset of growth is delayed, then a time offset can be introduced: $\theta(t) = 1 - e^{-\kappa(t-t_c)}$.[35,36]

First-order Langmuir kinetics have been extended to account for diffusion-limited kinetics,[37] second-order processes,[12,37] and intermolecular interactions.[30] When growth is limited by the diffusion of molecules from the bulk solution to the surface, one obtains the square-root time dependence associated with diffusive random walks:

$$\theta(t) = 1 - e^{-\sqrt{\kappa t}}\,, \tag{4}$$

The diffusion-limited Langmuir model successfully describes the adsorption kinetics of alkanethiol molecules on bare gold surfaces from very dilute solutions (<100 μM).[38] If the rate of adsorption is second-order in the thiol concentration, one obtains:

$$\theta(t) = 1 - \frac{1}{1+\kappa t}\,. \tag{5}$$

Second-order Langmuir adsorption kinetics have been used to describe ligand-exchange reactions on ligand-stabilized nanoparticles, in which the rate of the reaction is taken to depend on the concentration of the exchanging thiol both in solution and on the surface.[12]

The kinetics of nucleation and island growth were first modeled by Johnson, Mehl, Avrami, and Kolmogorov (JMAK) in the 1940s to describe metal alloy phase transformations.[39−42]

(28) Bain, C. D.; Whitesides, G. M. *J. Am. Chem. Soc.* **1989**, *111*, 7164−7175.
(29) Thomas, R. C.; Sun, L.; Crooks, R. M.; Ricco, A. J. *Langmuir* **1991**, *7*, 620−622.
(30) Dannenberger, O.; Buck, M.; Grunze, M. *J. Phys. Chem. B* **1999**, *103*, 2202−2213.
(31) Himmelhaus, M.; Eisert, F.; Buck, M.; Grunze, M. *J. Phys. Chem. B* **2000**, *104*, 576−584.
(32) Karpovich, D. S.; Blanchard, G. J. *Langmuir* **1994**, *10*, 3315−3322.
(33) Spinke, J.; Liley, M.; Schmitt, F. J.; Guder, H. J.; Angermaier, L.; Knoll, W. *J. Chem. Phys.* **1993**, *99*, 7012−7019.
(34) Langmuir, I. *J. Appl. Phys.* **1918**, *40*, 1361−1403.
(35) Eberhardt, A.; Fenter, P.; Eisenberger, P. *Surf. Sci.* **1998**, *397*, L285−L290.
(36) Schwartz, P.; Schreiber, F.; Eisenberger, P.; Scoles, G. *Surf. Sci.* **1999**, *423*, 208−224.
(37) Peterlinz, K. A.; Georgiadis, R. *Langmuir* **1996**, *12*, 4731−4740.
(38) Woodward, J. T.; Doudevski, I.; Sikes, H. D.; Schwartz, D. K. *J. Phys. Chem. B* **1997**, *101*, 7535−7541.
(39) Avrami, M. *J. Chem. Phys.* **1939**, *7*, 1103−1112.

The model has since been extended to address heterogeneous nucleation,[43] non-uniform island growth rates,[44,45] and boundary constraints[46−48] across a variety of physical systems including oxidizing metal surfaces,[49,50] graphite−diamond transformations,[51] and the crystallization of thin films[52] or proteins.[53] In this model, the rate of adsorption is proportional to the summed perimeter of all islands, yielding:

$$\theta(t) = 1 - e^{-(\kappa t)^n}, \qquad (6)$$

where κ is a rate constant.[39−41] The Avrami exponent n reflects the dimensionality of the system and the time dependence of the nucleation: $n = 2$ for a two-dimensional film, wherein nucleation proceeds rapidly to completion (site-saturated nucleation, JMAK2), and $n = 3$ in two dimensions if the nucleation rate is constant in time (constant-rate nucleation, JMAK3). In JMAK3, more nucleation sites become available as the transformation proceeds, such as in certain glass ceramics.[54] The exponentiation accounts for overlap between idealized non-interacting islands, whose growth curve is proportional to $(\kappa t)^n$.

Figure 3 shows least-squares fits of each kinetic model to the **C12** coverage versus exposure time for a 0.01 mM **C12** displacement solution. Only JMAK2 (eq 6 with $n = 2$) fits the data. A similar conclusion applies across the full range of all **C12** concentrations studied, from 0.01 to 1.0 mM, as shown in Figure 4.

The failure of the diffusion-limited models is, in fact, expected. Although such behavior is seen for *n*-alkanethiolate growth from very dilute solutions onto bare gold surfaces,[28] adsorption in our system is much slower (minutes as opposed to seconds), and the solution concentrations are much higher (millimolar as opposed to micromolar). The failure of Langmuir-based models, wherein adsorption is equally probable at all unoccupied sites, is consistent with the STM observation that adsorption begins at defect sites (i.e., not within the interiors of **AD** domains) and then proceeds at the **AD**−**C12** domain boundaries.[22] Rapid nucleation across these pre-existing active sites would then account for the success of JMAK2 over JMAK3. Although several elaborations upon JMAK2 (incorporating boundary effects or non-uniform growth rates) could be derived, such subtle distinctions are not resolved by the data.

The fits to JMAK2 also provide a measure of the displacement rate constant κ for each **C12** concentration. Figure 5 plots the log of κ for all experimental trials against the log of the **C12** solution concentration. The slope of 0.50 ± 0.05 suggests

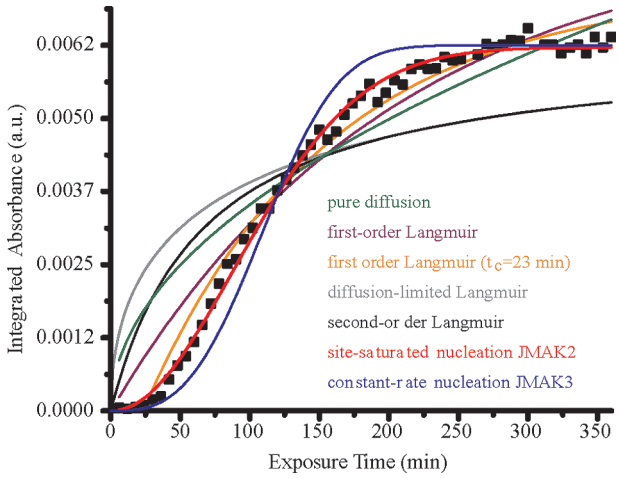

Figure 3. Representative 0.01 mM **C12** uptake curve with least-squares fits to pure diffusion (green), first-order Langmuir (purple), first-order Langmuir with an onset of growth at 23 min (orange), diffusion-limited Langmuir (gray), second-order Langmuir (black), site-saturated nucleation JMAK2 (red), and constant-rate nucleation JMAK3 (blue) models.

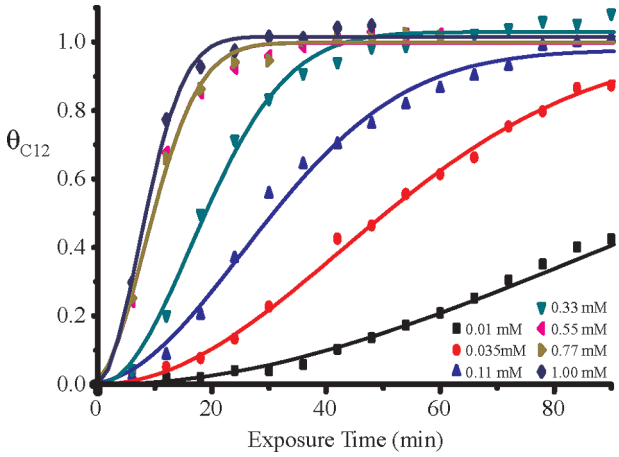

Figure 4. *n*-Dodecanethiolate monolayer formation by the displacement of an **AD** SAM as a function of concentration. Solid lines are least-squares fits based on the site-saturated nucleation model JMAK2 (eq 6 with $n = 2$).

that the displacement rate is proportional to the square-root of the **C12** solution concentration, assuming that the density of nucleation sites is roughly constant across all samples. This result is surprising, since insertion/displacement is expected to be a unimolecular process and a bimolecular process would yield a slope of 2, not 1/2. Half-order kinetics can arise, for example, when the displacement of Y by X actually proceeds by the decomposition of a predominant bimolecular state X_2 that generates X.

In addition to drawing specific conclusions regarding the relative quality of fits to different kinetic models, one can also analyze the displacement curves on a model-free basis to extract general conclusions regarding the number and character of any component subprocesses. Consider a general physical process as a composition of multiple subprocesses, each having a unique characteristic time scale or length scale, such as the growth of a tree across diurnal and annual cycles from a narrow smooth-skinned sapling to a wider mature state with regular cracks in its bark. When observing only a time-lapse movie of the tree's growth, one can immediately determine the frame rate and zoom factor: the faster cycle can be used as a clock to pace the slower

(40) Avrami, M. *J. Chem. Phys.* **1940**, *8*, 212−224.
(41) Avrami, M. *J. Chem. Phys.* **1941**, *9*, 117−184.
(42) Johnson, W. A.; Mehl, R. F. *Trans. Am. Inst. Min. Metall. Eng.* **1939**, *135*, 416−442.
(43) Weinberg, M. C.; Birnie, D. P.; Shneidman, V. A. *J. Non-Cryst. Solids* **1997**, *219*, 89−99.
(44) Shneidman, V. A.; Weinberg, M. C. *J. Non-Cryst. Solids* **1993**, *160*, 89−98.
(45) Weinberg, M.; Kapral, R. *J. Chem. Phys.* **1989**, *91*, 7146−7152.
(46) Jun, S.; Zhang, H. Y.; Bechhoefer, J. *Phys. Rev. E* **2005**, *71*, 011908.
(47) Kooi, B. J. *Phys. Rev. B* **2004**, *70*, 224108.
(48) Kooi, B. J. *Phys. Rev. B* **2006**, *73*, 054103.
(49) Holloway, P. H.; Hudson, J. B. *Surf. Sci.* **1974**, *43*, 123−140.
(50) Holloway, P. H.; Hudson, J. B. *Surf. Sci.* **1974**, *43*, 141−149.
(51) Okada, T.; Utsumi, W.; Kaneko, H.; Turkevich, V.; Hamaya, N.; Shimomura, O. *Phys. Chem. Miner.* **2004**, *31*, 261−268.
(52) Ruitenberg, G.; Petford-Long, A. K.; Doole, R. C. *J. Appl. Phys.* **2002**, *92*, 3116−3123.
(53) Baird, J. K.; Hill, S. C.; Clunie, J. C. *J. Cryst. Growth* **1999**, *196*, 220−225.
(54) Holand, W.; Rheinberger, V.; Schweiger, M. *Philos. Trans. R. Soc. A* **2003**, *361*, 575−588.

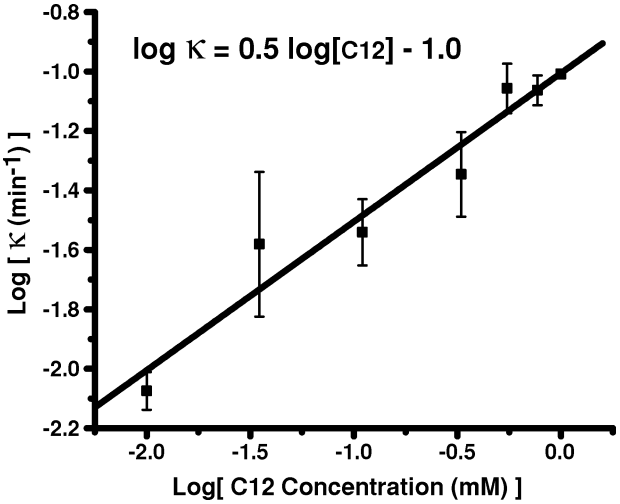

Figure 5. Displacement rate constant versus **C12** concentration on a logarithmic scale. The slope of 0.50 ± 0.05 implies that the rate constant is proportional to the square-root of the **C12** concentration.

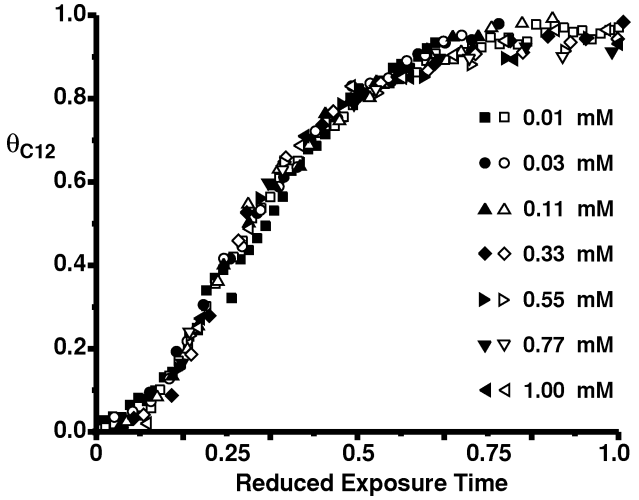

Figure 6. Plot of coverage versus reduced exposure time of two experimental runs at each **C12** concentration (0.01, 0.03, 0.11, 0.33, 0.55, 0.77, and 1.0 mM), showing collapse onto a universal curve.

process, and the finer details can be used to measure out the coarser features. However, if a physical process is governed by a single time scale (i.e., one rate constant) and a single length scale (i.e., a density of nucleation sites), then the physical system, considered in isolation, has no intrinsic clocks or rulers. By simply viewing a movie of ideal island nucleation and growth, one can determine neither the frame rate nor the zoom setting. In mathematical terms, the curves describing the kinetics of a scale-free process can be collapsed onto a *single universal curve* by a simple rescaling of the time and space (in this case, areal coverage) axes. In physical terms, from just the *shape* of a **C12** displacement curve, one can surmise nothing about the density of nucleation sites or the rate of displacement. In chemical terms, displacement is dominated solely by the rate of insertion at the island edge—were any other insertion processes to be active, with different dependences on solution concentration, then the displacement curves would have different shapes at different concentrations.

Figure 6 demonstrates, on a model-free basis, that the displacement of **AD** by **C12** is, to a good approximation, a scale-free process, governed by a single rate constant and a single characteristic length scale. Upon rescaling the time and coverage axes, the data across a 100-fold range of **C12** concentration collapse onto a single universal curve. For convenience, this rescaling uses the JMAK2 rate constants, but as mentioned above, this scale-free universal behavior is model-independent. The scale-free universal behavior suggests that the displacement of **AD** is dominated by a single physical process, edge insertion, across a 100-fold variation in solution concentration.

The importance of island growth in controlling the shape of the kinetic curves reflects the fact that displacement, adsorption, and desorption kinetics more generally are affected by the spatial structure of the growing phase. For example, desorption of small molecules from surfaces (e.g., alkanes from MgO[55,56]) is purely first-order if all molecules remaining on the surface are equally probably desorbed, but it may acquire an island growth component if molecules desorb preferentially from the edges of patches. These effects could be especially important if subtle features in desorption curves are used to fit detailed kinetic models with, e.g., temperature-dependent entropic contributions to pre-exponential factors in the Polanyi−Wigner equation.[55]

Why is it that **AD** SAMs are displaced fully by alkanethiols, but shorter-chain alkanethiols are only partially displaced by longer-chain alkanethiols, and does this distinction have larger relevance to the relation between lattice structure and kinetics for nucleation and growth of one phase within another? Generally, when one solid phase consumes another, whether by a structural phase transformation in an alloy or by a reaction such as oxidation at a surface or elsewhere, the lattices of the two phases are incompatible, meaning that lattice regularity is disrupted at the interface between the phases. This disruption tends to lower kinetic barriers against growth of the new phase at the interface. However, in SAMs, it is the solid substrate underneath that defines the lattice: for alkanethiol/alkanethiolate displacement on gold, the lattices of the two phases are *identical*: this situation is highly unusual in material phase transformations.[57] The interface between long- and short-chain alkanethiol SAMs can then be seamless, with no gaps to facilitate insertion of new longer-chain alkanethiols (at least after any pre-existing defect sites are filled). The free energy gain of enhanced cohesion in the new phase (due, in the SAM, to the greater length of the new alkyl chains) is then not sufficient to drive the reaction: the displacement of one thiol by another also requires ready access to the surface,[58] which is possible only if the two SAM lattices are incompatible. Adamantanethiolates, with a (7×7) unit cell, are incompatible with the alkanethiolate $(\sqrt{3} \times \sqrt{3})R30°$ unit cell; in this case the interface is disrupted and available for transverse attack by alkanethiols into the **AD** domain. This mechanism should apply more generally: phase transitions in systems wherein initial and final phases share an identical lattice can be kinetically hindered by the coherence of the interface between phases. In cases where lattice disruption at the interface is essential for overcoming

(55) Tait, S. L.; Dohnálek, Z.; Campbell, C. T.; Kaya, B. D. *J. Chem. Phys.* **2005**, *122*, 164707.
(56) Tait, S. L.; Dohnálek, Z.; Campbell, C. T.; Kaya, B. D. *J. Chem. Phys.* **2005**, *122*, 164708.
(57) In this regard, having two spatial dimensions is special: in three dimensions there is no orthogonal direction by which to define a consistent lattice externally, and in one dimension long-range order is strongly suppressed.
(58) Kolega, R. R.; Schlenoff, J. B. *Langmuir* **1998**, *14*, 5469−5478.

kinetic barriers, universal island growth kinetics, as described here, are expected to occur.

4. Conclusions

Our FTIR studies of the displacement of **AD** SAMs by **C12** on Au{111} demonstrate that displacement proceeds by site-saturation island nucleation and growth, not Langmuir kinetics nor any other model that has been previously used to describe the formation, exchange, or displacement of SAMs. We believe that the rapid and full displacement of **AD** SAMs is not unique and probably arises from a lattice mismatch with the **C12** domains, rationalizing why slow and incomplete displacement occurs in systems with similar packing structures. The kinetic curves collapse onto a universal curve upon rescaling, suggesting that the displacement process is purely geometrical.

Acknowledgment. We acknowledge support from the Air Force Office of Scientific Research, Defense Advanced Research Projects Agency, Office of Naval Research, and especially the National Science Foundation Center for Nanoscale Science (a MRSEC, DMR-0213623). T.J.M. is grateful for a graduate fellowship from the ACS Division of Analytical Chemistry sponsored by the Society of Analytical Chemists of Pittsburgh.

JA071116Z